THE JOURNAL OF PHYSICAL CHEMISTRY Letters

Letter

Cite This: J. Phys. Chem. Lett. 2018, 9, 2164−2169

pubs.acs.org/JPCL

# Direct Evidence of Exciton−Exciton Annihilation in Single-Crystalline Organic Metal Halide Nanotube Assemblies

Ying-Zhong Ma,*[,†] Haoran Lin,[‡] Mao-Hua Du,[§] Benjamin Doughty,[†] and Biwu Ma*[,‡,∥,⊥]

[†]Chemical Sciences Division, Oak Ridge National Laboratory, Oak Ridge, Tennessee 37831, United States

[‡]Department of Chemical and Biomedical Engineering, FAMU-FSU College of Engineering, Tallahassee, Florida 32310, United States

[§]Materials Science and Technology Division, Oak Ridge National Laboratory, Oak Ridge, Tennessee 37831, United States

[∥]Materials Science and Engineering Program, Florida State University, Tallahassee, Florida 32306, United States

[⊥]Department of Chemistry and Biochemistry, Florida State University, Tallahassee, Florida 32306, United States

Supporting Information

**ABSTRACT:** Excitons in low-dimensional organic−inorganic metal halide hybrid structures are commonly thought to undergo rapid self-trapping following creation due to strong quantum confinement and exciton−phonon interaction. Here we report an experimental study probing the dynamics of these self-trapped excitons in the single-crystalline bulk assemblies of 1D organic metal halide nanotubes, $(C_6H_{13}N_4)_3Pb_2Br_7$. Through time-resolved photoluminescence (PL) measurements at different excitation intensities, we observed a marked variation in the PL decay behavior that is manifested by an accelerated decay rate with increasing excitation fluence. Our results offer direct evidence of the occurrence of an exciton−exciton annihilation process, a nonlinear relaxation phenomenon that takes place only when some of the self-trapped excitons become mobile and can approach either each other or those trapped excitons. We further identify a fast and dominant PL decay component with a lifetime of ∼2 ns with a nearly invariant relative area for all acquired PL kinetics, suggesting that this rapid relaxation process is intrinsic.

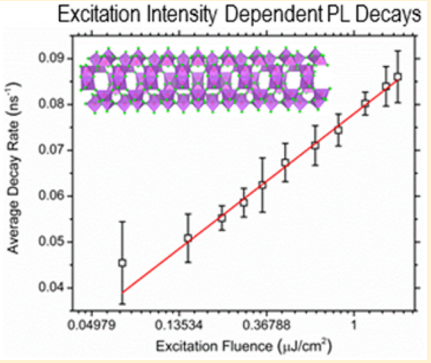


The exceptional structural tunability of organic−inorganic metal halide hybrids have motivated the development of various 0D, 1D, and 2D structures at the molecular level, in addition to the well-known 3D perovskite structure.[1−8] In these low-dimensional nanostructures, the basic building blocks, either individual metal halide octahedrons or their assemblies, are completely isolated from each other by organic ligands.[9] The strong spatial confinement and exciton−phonon interaction in these bulk assemblies of quantum confined structures lead to rapid exciton self-trapping, resulting in below-gap broadband emissions.[4,6,8,10−14] Because of the complete site isolation, the intrinsic properties of individual quantum confined nanostructures are reserved even after they form closely packed single-crystalline bulk assemblies. In other words, we can study the fundamental physics of the individual nanostructures directly in the macroscopic crystal form, as there is no interaction between them. This is significantly different from conventional packed assemblies of nanoscale materials that have strong interactions between each other, resulting in distinct properties for the assemblies and individual nanoscale materials.[15−17] A well known example is single-walled carbon nanotubes; their bundling has been shown to change not only optical spectral properties[18,19] but also electronic characteristics.[20]

Recently, we reported the synthesis and characterization of a single-crystalline bulk assembly of metal halide nanotubes, $(C_6H_{13}N_4)_3Pb_2Br_7$, in which six face-sharing metal halide dimers ($Pb_2Br_9^{5-}$) connect in corners to form 1D tubular structures.[9] A large array of these nanotubes is shown in Figure 1a. This unique 1D structure with strong quantum confinement and highly localized electronic states enables the formation of self-trapped excitons that give strongly Stokes-shifted broadband yellowish-white emission. Here we report further experimental study of the exciton dynamics in this bulk assembly of 1D organic metal halide nanotubes. Through picosecond time-resolved PL measurements on a macroscopic single crystal at different excitation intensities, we obtained direct evidence of the occurrence of an exciton−exciton annihilation process. This nonlinear annihilation process involves a pair of excitons whose interaction results in the disappearance of both excitons with the simultaneous induction of exciton population into an energetically resonant free exciton state ($FES_n$), and its subsequent rapid relaxation creates an exciton most likely in the lowest-lying state $FES_1$ owing to its excess energy (see Figure 1b). This process leads to

**Received:** March 12, 2018
**Accepted:** April 11, 2018
**Published:** April 11, 2018





DOI: 10.1021/acs.jpclett.8b00761
J. Phys. Chem. Lett. 2018, 9, 2164−2169

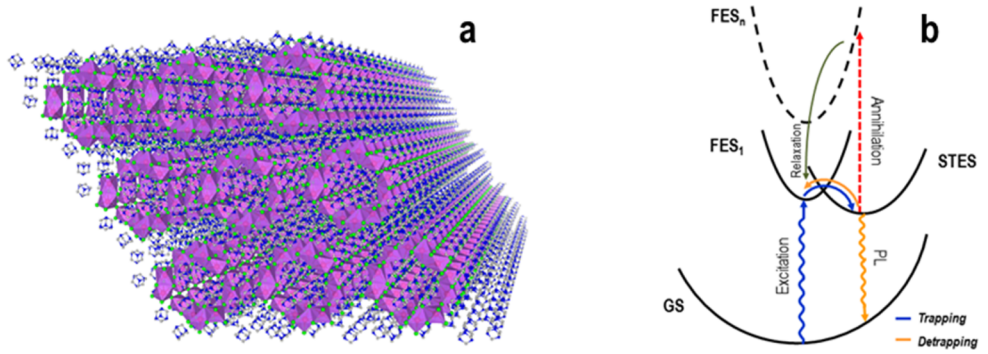


**Figure 1.** (a) View of the structure of $(C_6H_{13}N_4)_3Pb_2Br_7$ nanotube array, where red, green, blue, and gray denote lead, bromine, nitrogen, and carbon atoms, respectively. Purple polyhedra depict $PbBr_6$ octahedra and $Pb_2Br_9$ dimers, and hydrogen atoms are hidden for clarity. (b) Schematic energy level diagram of a nanotube involving exciton−exciton annihilation and exciton self-trapping and detrapping between the lowest-lying free exciton state ($FES_1$) and self-trapped exciton state (STES). GS and $FES_n$ denote the ground and a high-lying free exciton state, respectively.

significantly accelerated PL decays with increasing excitation intensity. Satisfactory description of the PL kinetics acquired at different excitation intensities was found to only be possible with a time-independent annihilation rate. We further identify a fast and dominant PL decay component with a lifetime of ∼2 ns that shows a nearly invariant relative area for all measured PL kinetics, suggesting that this rapid relaxation process is an intrinsic feature of these nanotubes. Our results not only offer new insights into the fundamental photophysics in these unique metal halide nanotube assemblies but also may serve as useful guidelines for their potential application or further improvement of their optical and electronic properties.

Time-resolved PL measurements were performed at 11 excitation intensities ranging from 0.07 to 1.65 $\mu J/cm^2$. As shown in Figure 2, all of the PL kinetics contain a sharp spike at

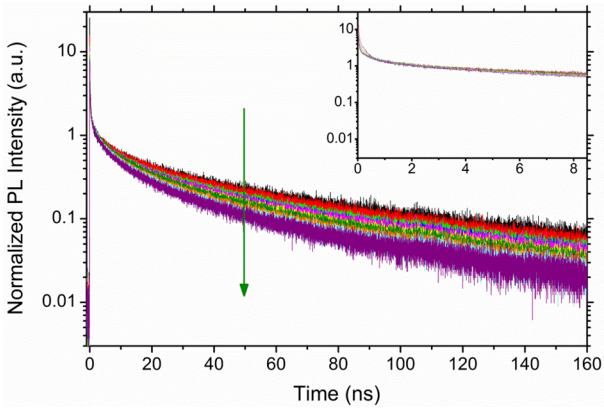


**Figure 2.** Time-resolved PL kinetics measured at 580 nm under different excitation intensities. The data are normalized at 2.36 ns, and the arrow depicts the direction of increasing intensity. The inset shows a portion of the same data at the early times, where the kinetics exhibit an indistinguishable decay behavior.

early times, which arises from stray excitation light scattering from the glass coverslips and possibly the sample consisting of several randomly positioned single crystals. The subsequent decays exhibit clearly multiexponential behavior and last for several hundreds of nanoseconds. To directly visualize if the change of excitation intensity will have any effect on these PL decays, we normalized all of the kinetics to 1 at 2.36 ns, where any influence from the initial spike has already become negligible. The raw data without normalization are shown in the Supplementary Figure S1. As can be seen in Figure 2, marked excitation intensity dependence is clearly evident, manifesting by an accelerated PL decay rate with increasing excitation fluence. This intensity dependence appears to be increasingly pronounced at time greater than ∼10 ns. The early portion of the kinetics exhibits an indistinguishable behavior within several nanoseconds after the initial spike but before the excitation intensity dependence becomes noticeable, as shown in the inset of Figure 2.

Quantitative analysis of the PL kinetics was performed to determine the lifetimes and associated amplitudes, and all of the fitting parameters are summarized in the Supplementary Table S1. We found that a satisfactory fit for each PL kinetic trace requires a model function of three exponential components in combination with an amplitude to account for the instantaneous response, that is, the initial spike, which is simply a multiple of the normalized IRF added to the convolved model curves. The first component is characterized by a lifetime (relative amplitude) ranging from ∼2.3 (45.3%) to ∼1.8 ns (53.6%) with increasing excitation intensity. The corresponding lifetimes (relative amplitudes) for the second and third components range from 14.1 (29.8%) to 11.0 ns (32.8%) and from 67.4 (24.9%) to 51.8 ns (13.7%), respectively. While with increasing excitation intensity all of the resolved lifetimes show roughly similar decreases with respect to their corresponding values at the lowest intensity, these changes alone do not represent the overall influence of the excitation intensity variation on the PL kinetics. This is because the intensity variation leads to changes of both these lifetimes and their associated amplitudes, and they may compensate each other when being treated as free variables in a fitting algorithm employing a complicated model function. In this regard, a more reliable assessment for the excitation intensity effect is to compare the relative areas associated with these decay components; such an area is simply equal to the product of the lifetime with its corresponding relative amplitude. As shown in the Supplementary Figure S2, the calculated relative area for the first component is essentially independent of the excitation intensity. In contrast, a clear intensity dependence is observed for the second component, whereas the third component shows the more prominent dependence on intensity with a factor of ∼2.5 reduction in relative area from the lowest to the highest intensity.

The presence of a fast decay component with a lifetime of ∼2 ns and a relative amplitude of ∼50% in all of the PL kinetics



DOI: 10.1021/acs.jpclett.8b00761
J. Phys. Chem. Lett. 2018, 9, 2164−2169

measured at different excitation intensities explains at least partially why the reported PL quantum efficiency of this material is relatively low compared with those of organic lead bromide hybrids with 3D, 2D-layered, and 1D-wire structures.[4,9,11] On the basis of the independence of its relative area on excitation intensity, we speculate that this rapid relaxation arises from the presence of a dark excitonic state. Assuming that the lowest-lying free exciton state, that is, the $FES_1$ in Figure 1b, and this dark state have same degeneracy, we can readily estimate that this dark state should lie roughly 140 $cm^{-1}$ below the $FES_1$ based on their approximately equal exciton population. Note that this estimate is based on the assumption that the time scale for thermalization is shorter than or comparable to the relaxation time of the $FES_1$ to the dark state, and the lifetime of the dark state is long compared with both these time scales, so that an exciton equilibrium can be established.[21] This intensity independence shown in the Supplementary Figure S2a further allows us to exclude defect or impurity trapping as the potential origin for this fast PL decay component, as such a trapping process should lead to a gradual increase in the relative area prior to the trap state saturation at high excitation intensities.[22]

The effect of excitation intensity on the PL decay kinetics can be also visualized by plotting the average decay rate, the inverse of the average lifetime, as a function of excitation intensity. As shown in the inset of Figure 3, the average decay rate increases

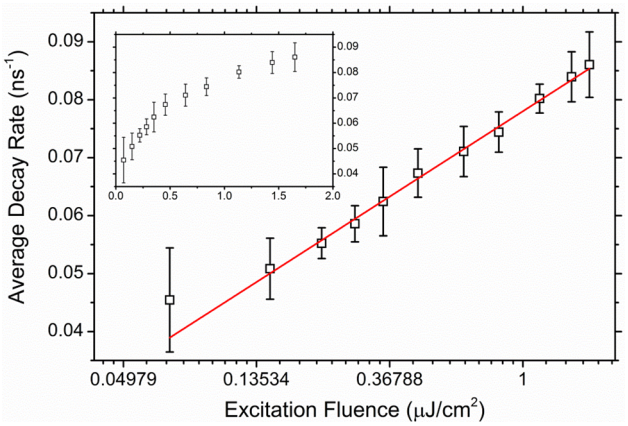


**Figure 3.** Plot of the average PL decay rate as a function of the natural logarithm of the excitation fluence. The error bars were calculated based on the errors of both the decay lifetimes and associated relative amplitudes estimated by the fitting algorithm, and the solid red line depicts a linear fit to the data. The inset shows the same data but plotted on a linear excitation intensity scale.

linearly with excitation intensity at low fluences but changes to a sublinear, saturation behavior with further increasing intensity. Upon changing the excitation fluence axis to natural logarithm scale, we found a clear linear dependence for most of the data points except the one obtained at the lowest excitation intensity.

The excitation-intensity-dependent PL decays shown in Figure 2 and the linear dependence of the average PL decay rate on the natural logarithm of the excitation intensity shown in Figure 3 are direct evidence of the occurrence of exciton−exciton annihilation in the nanotube assemblies.[23] This nonlinear process will open up an additional excited-state relaxation pathway, resulting in faster PL decays and higher decay rates with increasing excitation intensity. Further evidence of the occurrence of such an exciton−exciton annihilation process can be obtained by analyzing the time-resolved PL data using straightforward physical models that describe the time evolution of exciton population in the linear and nonlinear relaxation processes. This time evolution can be expressed by the following rate equation[23]

$$\frac{dn(t)}{dt} = -kn(t) - \frac{1}{2}\gamma(t)n^2(t) \quad (1)$$

where $n(t)$ is the exciton population in the STES, $k$ is the linear relaxation rate, and $\gamma(t)$ is the exciton−exciton annihilation rate. If the annihilation rate is time-independent, that is, $\gamma(t) = \gamma_0$, then an analytical solution of eq 1 can be readily derived

$$n(t) = \frac{n(0)e^{-kt}}{1 + n(0)\gamma_0 k^{-1}(1 - e^{-kt})} \quad (2)$$

where $n(0)$ is the initial exciton population. If the annihilation process in these 1D nanotubes is diffusion-limited, then the corresponding rate will be given by $\gamma(t) = \gamma_0/\sqrt{t}$ (ref 24) and the solution of eq 1 can be written as

$$n(t) = \frac{n(0)e^{-kt}}{1 + \frac{\gamma_0 n(0)}{\sqrt{\pi k}}\,\mathrm{erf}(\sqrt{kt})} \quad (3)$$

where erf() is the error function. Assuming that the quantum yield is independent of excitation intensity, the PL intensity at a given time $t$ would be proportional to $n(t)$. In this case, eqs 2 and 3 can be directly applied to analyze time-resolved PL data.

Analysis of the data collected at different excitation intensities was performed using a global algorithm and the normalized forms of eqs 2 and 3, that is, $n(t)/n(0)$, where $k$ and $\gamma_0$ were taken as global fitting parameters and a single set of their values that could best describe all PL kinetics was sought during the fitting. Furthermore, $n(0)$ was treated as a local parameter, and a separate value giving the best fit to each decay was determined. To avoid the complication arising from the initial spike and finite IRF, we omitted the very early portion of the PL kinetics in our data analysis until 2.36 ns, where all the kinetics are normalized. Given the much slower PL decays compared with IRF, no deconvolution procedure was applied in our global analyses. Representative results of our global analysis are shown in Figure 4, and the plots for the data acquired at the other nine excitation intensities can be found in the Supplementary Figure S3. A common feature for all of these plots is that the fits based on eq 2 are considerably better than those obtained using eq 3. On closer visualization, we further notice that the fits using eq 2 improve notably with increasing excitation intensity. This indicates that the annihilation process plays a minor role in the data acquired at low excitation intensity, and the single linear decay term in these cases is simply insufficient to capture the overall exciton relaxation dynamics. The parameters determined from the analysis are $k$ = 0.0058 $ns^{-1}$, and $\gamma_0 n(0)$ varies from 0.0073 to 0.143 $ns^{-1}$ with increasing excitation intensity. Note that only the $\gamma_0 n(0)$ values are given here because both $\gamma_0$ and $n(0)$ obtained from this analysis are relative numbers, as can be seen from eqs 2 and 3. In addition, the excitation intensity variation might alter both $n(0)$ and $\gamma_0$. To obtain absolute values for $\gamma_0$ and $n(0)$, one needs to independently determine the mean number of the excitons created in the nanotubes at different excitation intensities. This determination requires an accurate absorption


DOI: 10.1021/acs.jpclett.8b00761
J. Phys. Chem. Lett. 2018, 9, 2164−2169

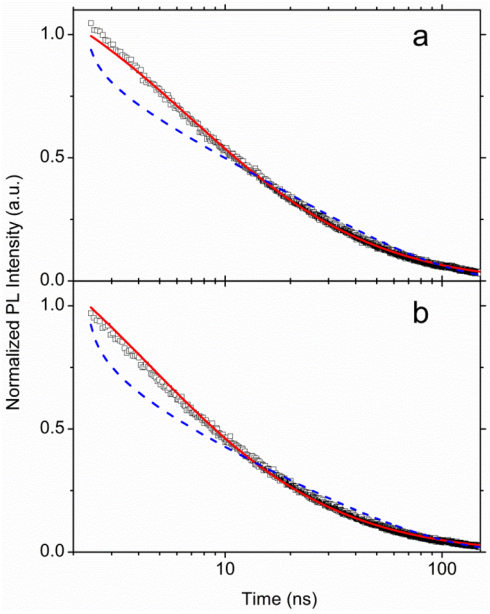


**Figure 4.** Results of global analysis for the time-resolved PL data collected at (a) 0.64 and (b) 1.65 $\mu J/cm^2$, respectively. The solid and dashed lines are the fits obtained using eqs 2 and 3, respectively. Note that the raw PL data were binned by every 10 data points to increase the signal-to-noise ratio.

cross-section for each nanotube and its number density at the excitation volume, which are unknown for the single-crystalline bulk assembly of these nanotubes. Because the absolute values for $n(0)$ at different excitation intensities are unknown, a similar analysis using the raw data shown in the Supplementary Figure S1 does not allow us to determine the absolute value of $\gamma_0$. Nevertheless, the key finding of our global analysis is that the PL kinetics, especially those measured at high excitation intensities, can be satisfactorily described by explicit consideration of exciton−exciton annihilation with a time-independent rate.

It should be noted, however, that the use of a time-independent annihilation rate seems to be intuitively in contradiction to the 1D structure of the nanotubes and the negligible interactions between them within their assemblies, as suggested by recent density functional theory calculations.[9] The calculated electronic band structure shows that both the conduction and the valence bands have significant dispersion along the 1D tube direction but are completely flat in the directions perpendicular to the axis of the tube. Therefore, the wave function overlap between adjacent tubes should be negligible, and under optical excitation, the excitons should be well confined within the 1D tube. This implies that exciton migration from one nanotube to another within the same assembly would be unlikely. This scenario is somewhat similar to the exciton diffusion in single-crystal copper-phthalocyanine (CuPc) nanowires.[25] Owing to the negligible interchain interactions, the exciton−exciton annihilation was previously revealed to involve intrachain excitons within 1D molecular stacks.[25−27] Consequently, we would expect a time-dependent annihilation rate and, in turn, better fits with eq 3 instead. We speculate that these seemingly unexpected results here stem most likely from rapid exciton self-trapping in these 1D nanotubes and detrapping at room temperature for some at shallow traps.[14] These detrapped excitons may, in turn, interact either between each other or with those that are still trapped, leading to an annihilation process that is not limited by exciton diffusion but instead is governed by the exciton detrapping and a combination of the subsequent migration of these detrapped excitons and the interactions between themselves and additionally with those trapped excitons. Given the relatively slow exciton dynamics observed for the 1D nanotubes, long-range excitation energy transfer might also occur, leading to an annihilation process involving excitons within the nanotube assemblies. While this would give rise to a time-independent annihilation rate, the negligible overlap between the absorption and emission spectra[9] make this unlikely. It is pertinent to mention that a greater than unity dimensionality of exciton motion has been previously found in semiconducting SWNTs.[28,29] The need for a time-independent annihilation rate in describing satisfactorily femtosecond fluorescence up-conversion and transient absorption kinetics acquired for structurally distinct 1D SWNTs was attributed to the occurrence of a rapid annihilation process involving coherently delocalized excitons.[30,31]

The results presented above offer new insights into the fundamental photophysics in these unique nanotube assemblies. First, although it has been well established that exciton self-trapping is particularly common in metal halide and rare-gas crystals,[32,33] which becomes much more pronounced at low-dimensional structures of these materials due to the increased level of electronic localization,[34,35] our observation of exciton−exciton annihilation provides direct evidence that some of the self-trapped excitons can become mobile at room temperature. As a result, the detrapped excitons can approach either each other or trapped ones to a distance smaller than the so-called reaction radius of the annihilation process to interact.[36] This implies that the energy needed for detrapping some of the self-trapped excitons is small and possibly comparable to the thermal energy at room temperature. This consideration is consistent with recent PL measurements at different temperatures, which suggests the formation of a thermal equilibrium between different trapped states as well as with the $FES_1$ at room temperature.[9,13] Second, the annihilation involving these trapped/detrapped excitons in the 1D nanotubes is remarkably distinct from those 1D exciton diffusion-limited annihilation phenomena observed in various 1D systems such as CuPc nanowires,[25] graphene nanoribbons,[37] and molecular J-aggregates,[38] where a time-dependent annihilation rate has been commonly found. Third, the nearly invariant relative area under the ~2 ns decay component for all acquired PL kinetics points to an intrinsic nature of this rapid relaxation instead of an externally influenced process such as exciton trapping at defects or impurity sites. On the basis of the presence of this fast decay component with a relative amplitude of ~50% in all the PL kinetics measured at different excitation intensities (see Supplementary Table S1), we propose the presence of a dark excitonic state that lies below the $FES_1$ state, leading to a branching of approximately half the exciton population from the free exciton state ($FES_1$ in Figure 1b) to the dark state. Such a low-lying dark state has been theoretically predicted and experimentally observed in semiconducting SWNTs.[21,39,40] To confirm the presence of such a dark state in these organic metal halide nanotubes, detailed calculations of electronic structure for the relevant excitonic states will be needed. Moreover, whether the excitons at the dark state can be involved in the annihilation process remains as an open question, and a definitive answer requires independent


DOI: 10.1021/acs.jpclett.8b00761
J. Phys. Chem. Lett. 2018, 9, 2164−2169

determination of their lifetimes using techniques such as transient absorption spectroscopy.

In summary, we have presented the results of time-resolved PL spectroscopic measurements on the bulk assemblies of 1D organic metal halide nanotubes, $(C_6H_{13}N_4)_3Pb_2Br_7$. The PL kinetics acquired at different excitation intensities exhibit a marked intensity-dependent decay behavior, manifested by an accelerated decay with increasing intensity. On the basis of the analysis of these PL kinetics with straightforward physical models, we conclude that the observed dependence arises from the occurrence of an exciton−exciton annihilation process in the nanotubes. The need for a time-independent annihilation rate to satisfactorily describe the PL decays is considered to reflect a distinct mechanism underlying this nonlinear process, which is limited not by exciton diffusion but instead by the exciton detrapping and subsequent interactions. We further identify a fast and dominant PL decay component with a lifetime of ∼2 ns, whose relative area appears nearly invariant for all PL kinetics acquired at different excitation intensities. This suggests an intrinsic nature for this fast relaxation, which is proposed to arise from exciton population branching to a low-lying dark state.

## EXPERIMENTAL METHODS

Time-resolved PL measurements were performed using a picosecond time-correlated single-photon-counting (TCSPC) technique.[41] The light source was an optical parametric amplifier (OPA) pumped by a 250 kHz femtosecond Ti:sapphire regenerative amplifier; its output centered at 692 nm was frequency-doubled using a 2 mm thick BBO crystal to generate the excitation pulse centered at 346 nm. The remaining fundamental laser light was removed using a short-pass filter. The excitation light was focused to ∼150 $\mu$m spot at the crystalline sample, which was sandwiched between two pieces of 1 mm thick microscope coverslips using a quartz lens. The selection of emission wavelength was accomplished using a bandpass filter with a center wavelength of 580 nm and a full width at half-maximum (fwhm) of 10 nm. The detection system includes an actively quenched single photon avalanche photodiode (PDM 50CT module, Micro Photon Devices) and a TCSPC module (PicoHarp 300, PicoQuant). A 8.0 ps channel time was chosen, and the polarization of the excitation beam was set to the magic angle (54.7°) with respect to an emission linear polarizer. Neutral density filters were used to attenuate the OPA output for excitation intensity control and to reduce the PL counts to eliminate pile-up artifacts that can occur at high excitation intensities.

Single decay analysis of the time-resolved PL data was performed by employing a least-squares deconvolution fitting algorithm (FluoFit, PicoQuant) with explicit consideration of the finite instrument response function (IRF). The IRF was acquired using a dilute suspension of coffee creamer in water through a 1 mm thick sample cell at the emission wavelength, which showed a fwhm of 67 ps. A reduced chi-squares ($\chi^2$) value was used to judge the quality of each fit.

## ASSOCIATED CONTENT

### Supporting Information

The Supporting Information is available free of charge on the ACS Publications website at DOI: 10.1021/acs.jpclett.8b00761.

Supplementary table summarizing the lifetimes, relative amplitudes, average lifetimes, and reduced chi-squares values extracted using a least-squares deconvolution fitting algorithm for the time-resolved PL kinetics measured at different excitation intensities; supplementary figures showing the raw data of the time-resolved PL kinetics without normalization, the relative areas under the PL decay curves for the fast, immediate and slow components as a function of excitation intensity, and the results of global analysis for the time-resolved PL data collected at nine different excitation intensities that are not included in Figure 4. (PDF)

## AUTHOR INFORMATION


### Corresponding Authors

*Y.-Z.M.: E-mail: may1@ornl.gov.
*B.M.: E-mail: bma@fsu.edu.

### ORCID

Ying-Zhong Ma: 0000-0002-8154-1006
Mao-Hua Du: 0000-0001-8796-167X
Benjamin Doughty: 0000-0001-6429-9329
Biwu Ma: 0000-0003-1573-8019


### Notes

The authors declare no competing financial interest.

## ACKNOWLEDGMENTS

The work at ORNL was supported by the U.S. Department of Energy, Office of Science, Basic Energy Sciences, Chemical Sciences, Geosciences, and Biosciences Division (Y.-Z.M. and B.D.), Materials Sciences and Engineering Division (M.-H.D.). H.L. and B.M. were supported by the Florida State University Energy and Materials Initiative and National Science Foundation (CHE 1664661 and DMR-1709116).

## REFERENCES


(1) Matsui, T.; Yamaguchi, A.; Takeoka, Y.; Rikukawa, M.; Sanui, K. Fabrication of Two-Dimensional Layered Perovskite $[Nh_3(Ch_2)_{12}nh_3]Pbx_4$ Thin Films Using a Self-Assembly Method. *Chem. Commun.* **2002**, 1094−1095.

(2) Wu, X.; Trinh, M. T.; Zhu, X.-Y. Excitonic Many-Body Interactions in Two-Dimensional Lead Iodide Perovskite Quantum Wells. *J. Phys. Chem. C* **2015**, *119*, 14714−14721.

(3) Dou, L.; Wong, A. B.; Yu, Y.; Lai, M.; Kornienko, N.; Eaton, S. W.; Fu, A.; Bischak, C. G.; Ma, J.; Ding, T.; et al. Atomically Thin Two-Dimensional Organic-Inorganic Hybrid Perovskites. *Science* **2015**, *349*, 1518−1521.

(4) Yuan, Z.; Zhou, C.; Tian, Y.; Shu, Y.; Messier, J.; Wang, J. C.; van de Burgt, L. J.; Kountouriotis, K.; Xin, Y.; Holt, E.; et al. One-Dimensional Organic Lead Halide Perovskites with Efficient Bluish White-Light Emission. *Nat. Commun.* **2017**, *8*, 14051.

(5) Zhou, C.; Tian, Y.; Wang, M.; Rose, A.; Besara, T.; Doyle, N. K.; Yuan, Z.; Wang, J. C.; Clark, R.; Hu, Y.; et al. Low-Dimensional Organic Tin Bromide Perovskites and Their Photoinduced Structural Transformation. *Angew. Chem., Int. Ed.* **2017**, *56*, 9018−9022.

(6) Zhou, C.; Lin, H.; Shi, H.; Tian, Y.; Pak, C.; Shatruk, M.; Zhou, Y.; Djurovich, P.; Du, M.-H.; Ma, B. A Zero-Dimensional Organic Seesaw-Shaped Tin Bromide with Highly Efficient Strongly Stokes-Shifted Deep-Red Emission. *Angew. Chem., Int. Ed.* **2018**, *57*, 1021−1024.

(7) Lin, H.; Zhou, C.; Tian, Y.; Siegrist, T.; Ma, B. Low-Dimensional Organometal Halide Perovskites. *ACS Energy Lett.* **2018**, *3*, 54−62.

(8) Zhou, C.; Lin, H.; Tian, Y.; Yuan, Z.; Clark, R.; Chen, B.; van de Burgt, L. J.; Wang, J. C.; Zhou, Y.; Hanson, K.; et al. Luminescent Zero-Dimensional Organic Metal Halide Hybrids with near-Unity Quantum Efficiency. *Chem. Sci.* **2018**, *9*, 586−593.




DOI: 10.1021/acs.jpclett.8b00761
J. Phys. Chem. Lett. 2018, 9, 2164−2169

(9) Lin, H.; Zhou, C.; Tian, Y.; Besara, T.; Neu, J.; Siegrist, T.; Zhou, Y.; Bullock, J.; Schanze, K. S.; Ming, W.; et al. Bulk Assembly of Organic Metal Halide Nanotubes. *Chem. Sci.* **2017**, *8*, 8400−8404.
(10) Dohner, E. R.; Hoke, E. T.; Karunadasa, H. I. Self-Assembly of Broadband White-Light Emitters. *J. Am. Chem. Soc.* **2014**, *136*, 1718−1721.
(11) Dohner, E. R.; Jaffe, A.; Bradshaw, L. R.; Karunadasa, H. I. Intrinsic White-Light Emission from Layered Hybrid Perovskites. *J. Am. Chem. Soc.* **2014**, *136*, 13154−13157.
(12) Hu, T.; Smith, M. D.; Dohner, E. R.; Sher, M.-J.; Wu, X.; Trinh, M. T.; Fisher, A.; Corbett, J.; Zhu, X.-Y.; Karunadasa, H. I.; et al. Mechanism for Broadband White-Light Emission from Two-Dimensional (110) Hybrid Perovskites. *J. Phys. Chem. Lett.* **2016**, *7*, 2258−2263.
(13) Smith, M. D.; Jaffe, A.; Dohner, E. R.; Lindenberg, A. M.; Karunadasa, H. I. Structural Origins of Broadband Emission from Layered Pb−Br Hybrid Perovskites. *Chem. Sci.* **2017**, *8*, 4497−4504.
(14) Smith, M. D.; Karunadasa, H. I. White-Light Emission from Layered Halide Perovskites. *Acc. Chem. Res.* **2018**, *51*, 619−627.
(15) Alivisatos, A. P. Semiconductor Clusters, Nanocrystals, and Quantum Dots. *Science* **1996**, *271*, 933−937.
(16) Mirkin, C. A.; Letsinger, R. L.; Mucic, R. C.; Storhoff, J. J. A DNA-Based Method for Rationally Assembling Nanoparticles into Macroscopic Materials. *Nature* **1996**, *382*, 607−609.
(17) Murray, C. B.; Kagan, C. R.; Bawendi, M. G. Synthesis and Characterization of Monodisperse Nanocrystals and Close-Packed Nanocrystal Assemblies. *Annu. Rev. Mater. Sci.* **2000**, *30*, 545−610.
(18) O'Connell, M. J.; Bachilo, S. M.; Huffman, C. B.; Moore, V. C.; Strano, M. S.; Haroz, E. H.; Rialon, K. L.; Boul, P. J.; Noon, W. H.; Kittrell, C.; et al. Band Gap Fluorescence from Individual Single-Walled Carbon Nanotubes. *Science* **2002**, *297*, 593−596.
(19) Arnold, M. S.; Green, A. A.; Hulvat, J. F.; Stupp, S. I.; Hersam, M. C. Sorting Carbon Nanotubes by Electronic Structure Using Density Differentiation. *Nat. Nanotechnol.* **2006**, *1*, 60−65.
(20) Ouyang, M.; Huang, J.-L.; Cheung, C. L.; Lieber, C. M. Energy Gaps in "Metallic" Single-Walled Carbon Nanotubes. *Science* **2001**, *292*, 702−705.
(21) Ma, Y.-Z.; Spataru, C. D.; Valkunas, L.; Louie, S. G.; Fleming, G. R. Spectroscopy of Zigzag Single-Walled Carbon Nanotubes: Comparing Femtosecond Transient Absorption Spectra with Ab Initio Calculations. *Phys. Rev. B: Condens. Matter Mater. Phys.* **2006**, *74*, 085402.
(22) Yamada, Y.; Yamada, T.; Shimazaki, A.; Wakamiya, A.; Kanemitsu, Y. Interfacial Charge-Carrier Trapping in $CH_3NH_3PbI_3$-Based Heterolayered Structures Revealed by Time-Resolved Photoluminescence Spectroscopy. *J. Phys. Chem. Lett.* **2016**, *7*, 1972−1977.
(23) van Amerongen, H.; Valkunas, L.; van Grondelle, R. *Photosynthetic Excitons*; World Scientific: London, 2000.
(24) Bunde, A.; Havlin, S. *Fractals and Disordered Systems*; Springer Verlag: Berlin, 1991.
(25) Ma, Y.-Z.; Xiao, K.; Shaw, R. W. Exciton−Exciton Annihilation in Copper-Phthalocyanine Single-Crystal Nanowires. *J. Phys. Chem. C* **2012**, *116*, 21588−21593.
(26) Gulbinas, V.; Chachisvilis, M.; Persson, A.; Svanberg, S.; Sundström, V. Ultrafast Excitation Relaxation in Colloidal Particles of Chloroaluminum Phthalocyanine: One-Dimensional Exciton-Exciton Annihilation. *J. Phys. Chem.* **1994**, *98*, 8118−8123.
(27) Gulbinas, V.; Chachisvilis, M.; Valkunas, L.; Sundström, V. Excited State Dynamics of Phthalocyanine Films. *J. Phys. Chem.* **1996**, *100*, 2213−2219.
(28) Ma, Y.-Z.; Stenger, J.; Zimmermann, J.; Bachilo, S. M.; Smalley, R. E.; Weisman, R. B.; Fleming, G. R. Ultrafast Carrier Dynamics in Single-Walled Carbon Nanotubes Probed by Femtosecond Spectroscopy. *J. Chem. Phys.* **2004**, *120*, 3368−3373.
(29) Ma, Y.-Z.; Valkunas, L.; Dexheimer, S. L.; Bachilo, S. M.; Fleming, G. R. Femtosecond Spectroscopy of Optical Excitations in Single-Walled Carbon Nanotubes: Evidence for Exciton-Exciton Annihilation. *Phys. Rev. Lett.* **2005**, *94*, 157402.
(30) Valkunas, L.; Ma, Y.-Z.; Fleming, G. R. Exciton-Exciton Annihilation in Single-Walled Carbon Nanotubes. *Phys. Rev. B: Condens. Matter Mater. Phys.* **2006**, *73*, 115432.
(31) Ma, Y.-Z.; Graham, M. W.; Fleming, G. R.; Green, A. A.; Hersam, M. C. Exciton Dephasing in Semiconducting Single-Walled Carbon Nanotubes. *Phys. Rev. Lett.* **2008**, *101*, 217402.
(32) Williams, R. T.; Song, K. S. The Self-Trapped Exciton. *J. Phys. Chem. Solids* **1990**, *51*, 679−716.
(33) Georgiev, M.; Mihailov, L.; Singh, J. Exciton Self-Trapping Processes. *Pure Appl. Chem.* **1995**, *67*, 447−456.
(34) Ishida, K. Self-Trapping Dynamics of Excitons on a One-Dimensional Lattice. *Z. Phys. B: Condens. Matter* **1997**, *102*, 483−491.
(35) Wu, X.; Trinh, M. T.; Niesner, D.; Zhu, H.; Norman, Z.; Owen, J. S.; Yaffe, O.; Kudisch, B. J.; Zhu, X.-Y. Trap States in Lead Iodide Perovskites. *J. Am. Chem. Soc.* **2015**, *137*, 2089−2096.
(36) Barzda, V.; Gulbinas, V.; Kananavicius, R.; Cervinskas, V.; van Amerongen, H.; van Grondelle, R.; Valkunas, L. Singlet-Singlet Annihilation Kinetics in Aggregates and Trimers of LHCII. *Biophys. J.* **2001**, *80*, 2409−2421.
(37) Soavi, G.; Dal Conte, S.; Manzoni, C.; Viola, D.; Narita, A.; Hu, Y.; Feng, X.; Hohenester, U.; Molinari, E.; Prezzi, D.; et al. Exciton−Exciton Annihilation and Biexciton Stimulated Emission in Graphene Nanoribbons. *Nat. Commun.* **2016**, *7*, 11010.
(38) Marciniak, H.; Li, X.-Q.; Würthner, F.; Lochbrunner, S. One-Dimensional Exciton Diffusion in Perylene Bisimide Aggregates. *J. Phys. Chem. A* **2011**, *115*, 648−654.
(39) Spataru, C. D.; Ismail-Beigi, S.; Capaz, R. B.; Louie, S. G. Theory and Ab Initio Calculation of Radiative Lifetime of Excitons in Semiconducting Carbon Nanotubes. *Phys. Rev. Lett.* **2005**, *95*, 247402.
(40) Zhao, H.; Mazumdar, S. Electron-Electron Interaction Effects on the Optical Excitations of Semiconducting Single-Walled Carbon Nanotubes. *Phys. Rev. Lett.* **2004**, *93*, 157402.
(41) Ma, Y.-Z.; Shaw, R. W.; Yu, X.; O'Neill, H. M.; Hong, K. Excited-State Dynamics of Water-Soluble Polythiophene Derivatives: Temperature and Side-Chain Length Effects. *J. Phys. Chem. B* **2012**, *116*, 14451−14460.


DOI: 10.1021/acs.jpclett.8b00761
*J. Phys. Chem. Lett.* 2018, 9, 2164−2169